Hindawi
Advances in Civil Engineering
Volume 2020, Article ID 8894286, 13 pages
https://doi.org/10.1155/2020/8894286

Research Article

Design and Verification of a Deep Rock Corer with Retaining the In Situ Temperature

Zhiqiang He,[1,2] Heping Xie,[1,2] Mingzhong Gao,[1,2] Ling Chen,[3] Bo Yu,[3] Yunqi Hu,[3] and Jianping Yang[4]

[1]*State Key Laboratory of Hydraulics and Mountain River Engineering, College of Water Resource and Hydropower, Sichuan University, Chengdu 610065, China*
[2]*Guangdong Provincial Key Laboratory of Deep Earth Sciences and Geothermal Energy Exploitation and Utilization, Institute of Deep Earth Sciences and Green Energy, College of Civil and Transportation Engineering, Shenzhen University, Shenzhen 518060, China*
[3]*School of Mechanical Engineering, Sichuan University, Chengdu 610065, China*
[4]*College of Polymer Science and Engineering, Sichuan University, Chengdu 610065, China*

Correspondence should be addressed to Ling Chen; chenlingscu@scu.edu.cn

Received 24 July 2020; Revised 22 August 2020; Accepted 31 August 2020; Published 15 September 2020

Academic Editor: Fengqiang Gong

Deep rock is always under high-temperature conditions. However, traditional coring methods generally have no thermal insulation design, which introduces large deviations in the guidance required for resource mining. Thus, a thermal insulation design that utilizes active and passive thermal insulation was proposed for deep rock corers. The rationale behind the active thermal insulation scheme was to maintain the in situ core temperature through electric heating that was controlled by using a proportional-integral-derivative (PID) chip. Graphene heating material could be used as a heating material for active thermal insulation through testing. In regard to the passive thermal insulation scheme, we conducted insulation and microscopic and insulation effectiveness tests for hollow glass microsphere (HGM) composites and SiO_2 aerogels. Results showed that the #1 HGM composite (C_1) had an excellent thermal insulation performance (3 mm thick C_1 can insulate to 82.6°C), high reflectivity (90.02%), and wide applicability. Therefore, C_1 could be used as a passive insulation material in deep rock corers. Moreover, a heat transfer model that considered multiple heat dissipation surfaces was established, which can provide theoretical guidance for engineering applications. Finally, a verification test of the integrated active and passive thermal insulation system (graphene heating material and C_1) was carried out. Results showed that the insulating effect could be increased by 13.3%; thus, the feasibility of the integrated thermal insulation system was verified. The abovementioned design scheme and test results provide research basis and guidance for the development of thermally insulated deep rock coring equipment.

1. Introduction

Deep mining has become more common owing to the exhaustion of shallow mineral resources [1], and many disasters have occurred in deep engineering [2]. For example, current coal mining has reached 1 500 m in depth, geothermal exploitation has reached a depth of over 3 000 m, the depth for ferrous metal mining is over 4 350 m, and the depth for oil and gas development is 7 500 m [3, 4]. Also, deep engineering, such as coal mining, urgently needs theoretical guidance [5, 6]. Deep rock is always under high ground stress and high-temperature conditions, which is very different from shallow rocks [7–10]. Temperature is an important factor that affects rock mechanics and other properties. Also, coal mining that gradually develops deeper is affected by temperature. Therefore, many scholars have conducted research on the mechanical characteristics of coal, the gas adsorption/desorption behavior, and the seepage laws influenced by temperature. Regarding the mechanical characteristics of coal, existing studies have shown that as the temperature increases, the strength of coal decreases [11–14]. In the study of the gas adsorption/

desorption behavior, relevant scholars believe that gas adsorption decreases with increasing temperature [15–18]. However, the relationship between gas seepage and temperature is complicated, and there is no unified understanding [19–21]. Therefore, as the temperature increases, the mechanical characteristics of coal, the gas adsorption/desorption behavior, and the seepage laws will change. Taking these properties of rock at a normal temperature as the properties of deep rock will introduce large deviations to the deep engineering. Therefore, temperature is particularly important as one of the in situ conditions for deep rock. Scientific drilling has become an indispensable and important means for human beings to solve major problems related to resources, disasters, and the environment. However, due to the inability to retain the in situ temperature in traditional deep rock coring on the land, the distortion of core temperature will result in an incomplete scientific acquisition of the in situ core mechanical behavior and gas phase information. Therefore, it is necessary to develop thermally insulated coring equipment for deep rock and provide a basis for subsequent tests.

The main focus of deep coring on the land is still on drilling technology. Only deep-sea samplers have taken the lead in coring technology with retaining in situ conditions of sediments [22]. However, these devices are mainly designed for retaining pressure, and most of them do not consider thermal insulation design. Instead, the core is placed in a cooler when the devices are raised to the ground, such as the Multiple Autoclave Corer (MAC) and the Dynamic Autoclave Piston Corer (DAPC) [23]. Only a few deep-sea samplers include thermal insulation technology. Both the Pressure Temperature Core Sampler (PTCS) and the High Pressure Temperature Corer (HPTC) adopt a double-layer inner tube for thermal insulation [24–26]. The Pressure and Temperature Preservation System (PTPS) developed by Zhu et al. uses a vacuum layer with the inner surface sprayed with a thermal insulation material and the outer surface sprayed with an anti-UV coating [27]. The fidelity coring device developed by Zhejiang University adopts a thermal insulation coating [28–30]. However, the insulation measures of the abovementioned corers are passive thermal insulation (reducing the heat dissipation of the core), and no active thermal insulation measures are taken (retaining the in situ temperature), thereby resulting in the core temperature still decreasing. In addition, it is very different from thermal insulation measures of seafloor sediments, where deep rock is always under high-temperature conditions. The purpose of coring with thermal insulation is to prevent the core temperature from decreasing. Therefore, the existing thermal insulation technology cannot be directly applied to coring equipment on the land for deep rock. Thus, thermal insulation technology for deep rock coring requires further exploration [31].

A scheme for thermally insulated coring technology (150°C insulation target) for deep rock was designed based on concept of the in situ fidelity coring system [31]. Laboratory experiments were carried out with a combination of active and passive thermal insulation as the research idea. From the principle of the active thermal insulation scheme, test results showed that graphene heating material could be used as a heating material. Passive thermal insulation and microscopic tests were carried out. Results show that C_1 can be used as passive thermal insulation. Moreover, a heat transfer model was established, which could provide theoretical guidance for engineering applications. Finally, a verification test was carried out on the combination of the graphene heating material and C_1, as an integrated active and passive thermal insulation system. Thus, the feasibility and superiority of the thermal insulation scheme for coring technology were verified.

2. Thermal Insulation Scheme for Deep Rock Coring Technology

In view of the high-temperature conditions of deep rock, an active thermal insulation design uses electric heating to retain the temperature. Using a special battery as an energy source, the core temperature is collected by the sensor and fed back to PID chip. Finally, the PID chip controls the electric heating material to compensate for the decreasing temperature of the core in real time, as shown in Figure 1.

Moreover, passive thermal insulation is designed to reduce the influence of the ambient temperature and the energy consumption of the active thermal insulation. There are three ways of heat transfer: thermal conduction, thermal convection, and thermal radiation. The core in the corer mainly dissipates heat through the metal cabin wall by thermal conduction, resulting in a decrease in temperature. Materials with low thermal conductivity can effectively reduce heat dissipation. Thus, it is necessary to combine a material with low conductivity with the cabin wall surface to reduce the magnitude of the temperature drop.

As shown in Figure 2, according to the abovementioned ideas, a deep rock corer which adopts a combination of active and passive thermal insulation is designed.

3. Design of the Active Thermal Insulation Scheme

The heating material of the active thermal insulation is the key part. Therefore, heating material optimization tests were performed first. To satisfy the need for fast heating and high-temperature resistance, a graphene heating material, silicone heating film, and polyimide heating film were tested for comparison (see Figure 3). The graphene heating material was 10 μm of graphene attached to an aluminum plate, and ceramics were used as insulation. The silicone heating film was warmed up by a heating wire, and the outer silica gel was waterproof. The polyimide heating film was an electric heater, and the outer material was polyimide. Because a battery-powered scheme was adopted, a 12 V power supply was used in the laboratory to simulate the engineering conditions.

To observe the heating characteristics of the three materials in real time, temperature sensors were pasted on the surface, and the process for increasing temperature was recorded. As shown in Figure 4, the graphene heating material has good thermal conductivity, exhibiting the

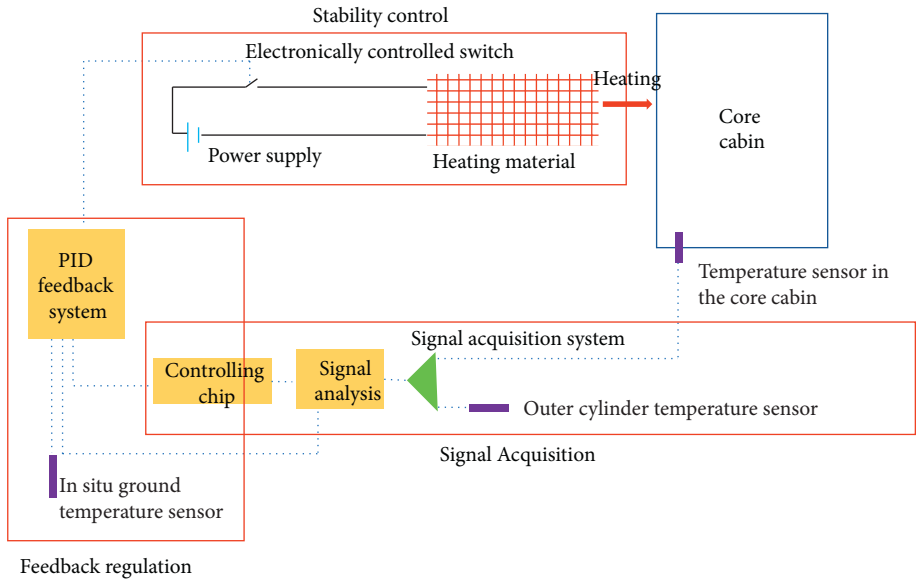

Figure 1: Schematic diagram of the active thermal insulation system.

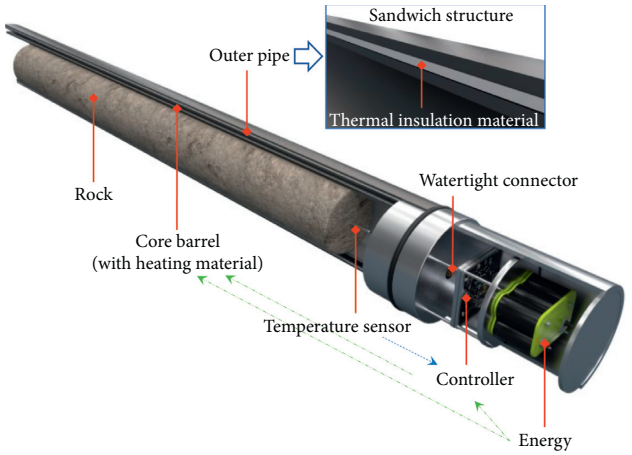

Figure 2: Scheme of thermally insulated coring technology for deep rock.

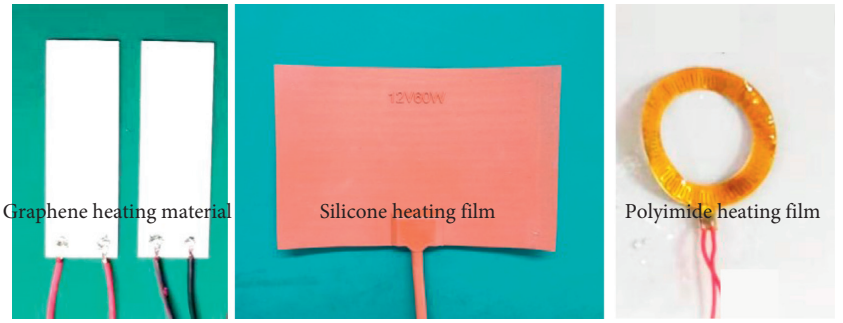

Figure 3: Active heating materials.

maximum heating rate and lowest thermal inertia. The temperature increases rapidly in a short period of time, and there is no tendency of slowing down. The polyimide heating film also has a smaller thermal inertia and faster cooling rate; however, it is not very waterproof. The outer silica gel of the silicone heating film increases its waterproofness but slows the heating rate. In engineering, it is necessary to have a quick response to temperature decreases in the core; thus, the heating material must have a small thermal inertia. Only the graphene heating material reaches 150°C with a 12 V

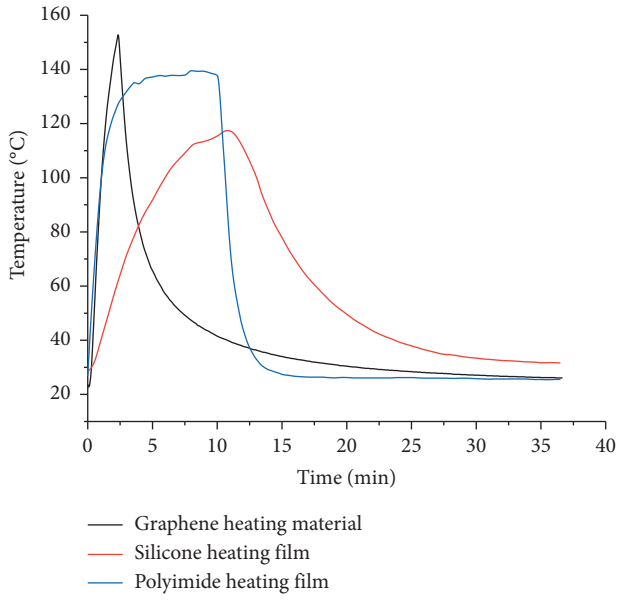

Figure 4: Heating characteristics of the three heating materials.

power supply. Therefore, considering the test results and working conditions, for example, the presence of water in deep rock, the graphene heating material is the best choice for the active thermal insulation.

To verify the characteristics of the heating material and its feasibility in the active thermal insulation scheme, the following experiment was designed. Four identical graphene heating materials were connected, and the heating area was the same as that of the silicone heating film (see Figure 5). The graphene and silicone heating film were used to heat water from room temperature to 80°C and, then, keep the temperature constant in the container with a 12 V power supply. The water temperature was monitored, and the voltage and current were recorded at the same time. The recorder used in the test had a PID chip and could also record data.

As shown in Figure 6, the silicone heating film needs 41.5 min to heat the water to 80°C, while the graphene heating material needs 13.5 min. Moreover, the energy consumption is 87 503.33 and 119 702.27 J for the graphene and silicone heating films, respectively. The graphene heating material reduces the time by 28.5 min and the energy consumption by 32198.94 J, advancing the possibility for a battery-powered scheme in engineering. At the retaining temperature stage, because of the instant feedback of the sensors and the real-time control of the PID, the graphene heating material can adjust the water temperature so that it remains 80°C with only slight fluctuations. These experimental results verified the heating effect of the graphene heating material and its feasibility as an active thermal insulation solution.

4. Design of the Passive Thermal Insulation Scheme

4.1. Passive Thermal Insulation Material Properties Research and Optimization. Passive thermal insulation schemes should choose materials with low thermal conductivity. The

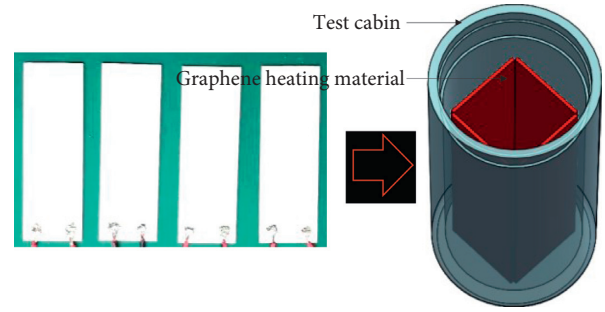

Figure 5: Graphene heating material in the heating water experiment.

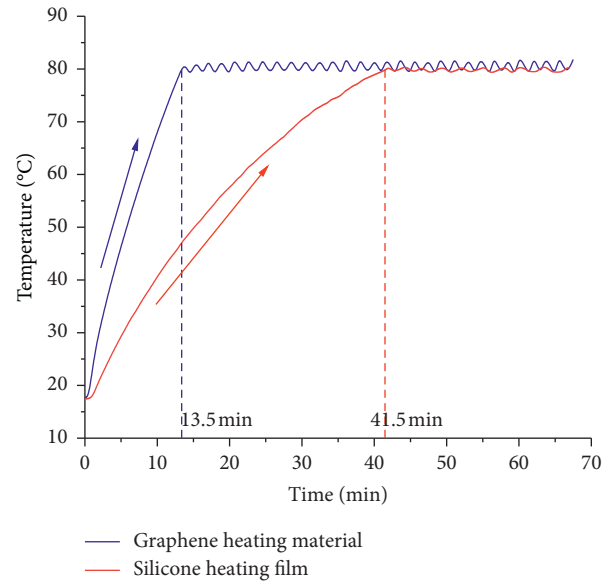

Figure 6: Water warming experiments with two different heating materials.

corer size limits the thickness of the insulation material. Therefore, the material should have very low thermal conductivity and stable chemical characteristics and is heat-tolerant and waterproof. There are many types of insulation materials, and after filtering, the SiO_2 aerogel and HGM were chosen.

The SiO_2 aerogel is a typical material with high porosity, low density, and very low thermal conductivity [32, 33], whereas the hollow structure of HGM insulates heat [34–36]. HGMs and the aerogel are widely applied. Therefore, these two materials were tested in the laboratory to choose the material with better heat insulation performance and, thus, better suitability for this engineering problem.

4.2. Insulation Tests. The fibre and adhesive are always added in the abovementioned materials when applied in engineering [32,37]. For the three HGM composites (named C_1, C_2, and C_3) and two aerogel felt materials, insulation tests were performed.

The HGM composites were applied to a copper plate surface, and the aerogel felt material was pasted on. The thickness was controlled to 1, 2, 3, and 4 mm, and the temperature of the muffle furnace was set to 150, 200, and 250°C. The samples were set on the opening of the muffle furnace (coating was placed outward), and the temperature change of the coating was recorded (see Figure 7).

Among the various tested thicknesses, the 1 and 2 mm thickness tests used aerogel felt-kono, while the 3 mm thickness tests used aerogel felt-nano, and the 4 mm thickness tests did not use aerogel felt, as shown in Figure 8.

A portion of the test results is shown in Figure 9. The temperature of the material on the plate increases gradually and, then, becomes stable. However, there are some differences in the coating process under different conditions. The results show that C_1, C_3, and the aerogel felt have better thermal insulation properties. For example, materials with thicknesses of 3 mm insulate to 82.6, 80.9, and 77.1°C, while the temperature of the muffle furnace is 150°C. C_1 and C_3 have better insulation properties than C_2. When the insulation thickness is thin, the coating results in poor uniformity. Therefore, the insulation properties of C_3 are better than those of C_1, and when the thickness increases, the properties of the two are almost the same. The insulation properties of aerogel felts with different thicknesses have some differences; furthermore, they require paste and easily drop powder during operation. Therefore, the applicability and operability of aerogel felts are limited in engineering. As a result, C_1 and C_3 were chosen for further comparison tests.

5. Microscopic Tests

To study the microcharacteristics of C_1 and C_3, microscopic tests were developed. Three HGM composite powders dried under natural conditions for 48 hours were sampled, as shown in Figure 10.

There are three heat transfer mechanisms of hollow microspheres: (1) solid heat conduction, (2) surface thermal radiation between adjacent hollow particles, and (3) thermal convection of air in HGM. When the diameters of the microspheres are less than 4 mm, there is no natural thermal convection in the internal air.

The scanning electron microscope (SEM) results of the three materials are shown in Figure 11. The diameters of the microspheres are 10–100 μm; thus, thermal convection should not be considered.

Microspheres increase the porosity and decrease the heat transfer of solids, resulting in a good insulation performance. C_2 may be more brittle because a large number of the microspheres broke. Thus, the decreasing porosity of C_2 results in a poor insulation performance.

The reflectance of materials to infrared light is shown in Figure 12. All three materials exhibit high reflectance to infrared light, and the reflectivity of the C_1 material is the highest, reaching 90.02% on average. Therefore, C_1 can better prevent external heat transfer in the form of thermal radiation. Additionally, for solids and liquids, a low absorption capacity results in high reflection ability [38]; for general objects, the absorption rate equals its reflection rate. The C_1 material has a low reflection rate, thereby reducing the heat loss of radiation to the outside world.

Finally, according to the comparison and analysis of the abovementioned optimization test results of the insulation materials, C_1 is selected as the passive thermal insulation material.

5.1. Passive Thermal Insulation Effectiveness Test. To provide guidance for engineering applications, it is necessary to test the effectiveness of the passive thermal insulation materials. The core cabin was simplified and processed as a small test cabin, as shown in Figure 13. The material was 304 stainless steel.

As shown in Figure 14, the insulation material was coated evenly on the surface of the small test cabin. The cabin was filled with L-QD350 thermal oil, which is conducive to temperature uniformity. The cabin was placed in the oven (150°C). After the temperature in the cabin reached 150°C, it was cooled naturally to room temperature.

The SiO_2 aerogel felt has a good thermal insulation performance. However, due to its limited applicability and operability, the SiO_2 aerogel coating and C_1 were used to conduct the next tests. The average thickness was 3 mm.

As shown in Figure 15, due to the effect of the thermal insulation material, the rate of temperature increase in the cabin with the thermal insulation material is significantly lower than that of the blank cabin at the heating stage. The initial cooling rates are 1.286, 1.287, and 1.484°C/min in the cabin coated by C_1, the SiO_2 aerogel coating, and the blank, respectively. In general, C_1 shows a good thermal insulation effect at both stages. It can not only reduce the disturbance caused by the ambient temperature change but also reduce the magnitude of the in situ temperature drop of the core. Therefore, C_1 can be used as a passive thermal insulation material in the corer.

6. Proposal of the Heat Transfer Model and the Integration of the Thermally Insulated Coring Test System

6.1. Heat Transfer Model of the Passive Thermal Insulation. Establishing a passive thermal insulation heat transfer model can provide theoretical guidance for the integration of thermal insulation systems and engineering applications. First, the thermal conductivity of C_1 is measured, as shown in Figure 16. The thermal conductivity gradually increases with increasing temperature and shows a good linear relationship:

$$\lambda C = 1.02e^{-4}T + 0.03427, \quad (1)$$

where λ_C is the thermal conductivity, W/(m·°C), and T is the average temperature, °C.

According to the simplified model of the small test cabin shown in Figure 17, a heat transfer model of the passive thermal insulation is established based on the transient thermal conduction theory [38]. Thus, the temperature change in the cabin is obtained.

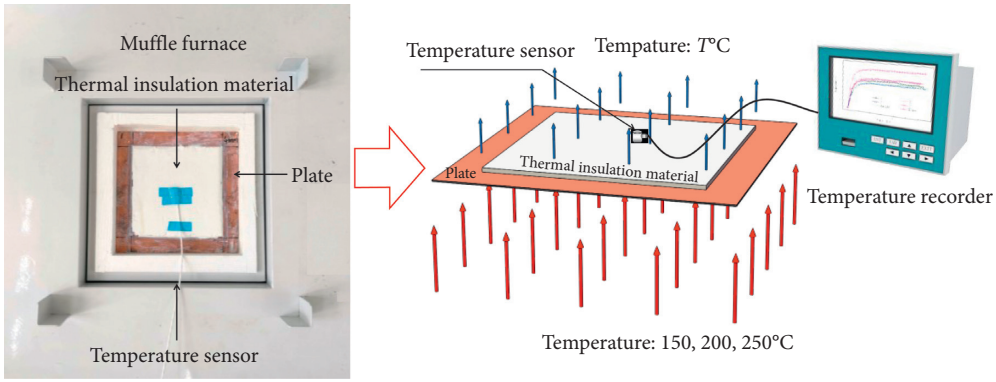

Figure 7: Insulation performance test.

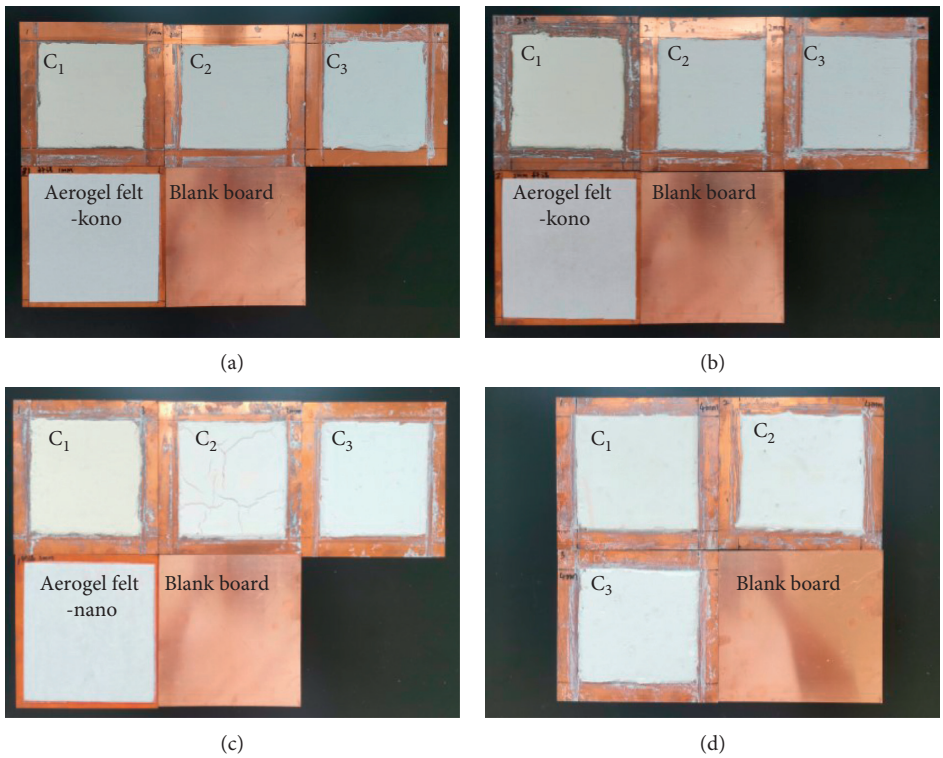

Figure 8: Tests plates. (a) Sample with 1 mm thickness. (b) Sample with 2 mm thickness. (c) Sample with 3 mm thickness. (d) Sample with 3 mm thickness.

The radial thermal resistance R_1 of the cabin wall, while considering thermal convection and thermal conduction, is shown as follows:

$$R_1 = \frac{1}{2\pi r_{g1} l h_f} + \frac{\ln\left(r_{g2}/r_{g1}\right)}{2\pi l \lambda_g} + \frac{\ln\left(r_c/r_{g2}\right)}{2\pi l \lambda_c} + \frac{1}{2\pi r_c l h_a}, \quad (2)$$

where R_1 is the radial thermal resistance of the cabin wall, °C/W; r_{g1}, r_{g2}, r_c are the cabin inner diameter, cabin outer diameter, and thermal insulation material outer diameter, respectively, m; λ_g and λ_c are the thermal conductivity of the cabin wall and insulation materials, W/(m·°C), and λ_g is set to 16.27 W/(m·°C); and h_f and h_a are the convective heat transfer coefficient of the internal fluid and the inner surface of the cabin wall, the thermal insulation material, and the ambient environment, respectively, which is set to 150 and 6.5 W/(m·°C), respectively.

Considering that the model height is relatively small, the thermal resistances of the upper and lower ends are calculated, as shown in the following equations:

$$R_2 = \frac{1}{h_f \pi r_{g1}^2} + \frac{\delta_u}{\lambda_g \pi r_{g1}^2} + \frac{\delta_c}{\lambda_c \pi r_{g1}^2} + \frac{1}{h_a \pi r_{g1}^2}, \quad (3)$$

$$R_3 = \frac{1}{h_f \pi r_{g1}^2} + \frac{\delta_d}{\lambda_g \pi r_{g1}^2} + \frac{\delta_c}{\lambda_c \pi r_{g1}^2} + \frac{1}{h_a \pi r_{g1}^2}, \quad (4)$$

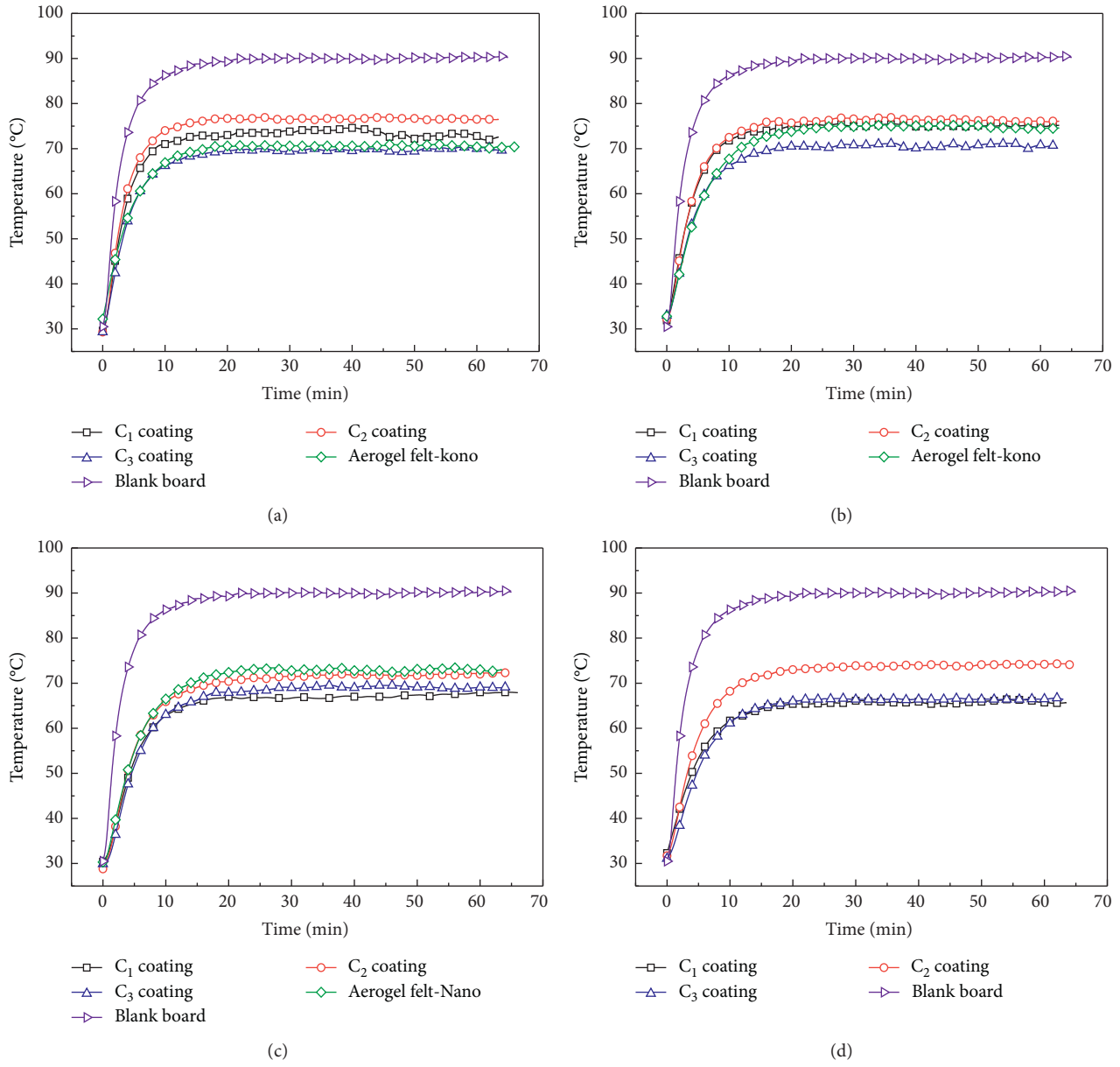

Figure 9: Insulation properties of the different materials. (a) 1 mm-150°C. (b) 2 mm-150°C. (c) 3 mm-150°C. (d) 4 mm-150°C.

Figure 10: Microscopic test samples.

where R_2 and R_3 are the thermal resistances of the upper and lower ends of the cabin wall, °C/W; δ_u, δ_d, and δ_c are the thicknesses of the upper and lower ends and the thermal insulation material, respectively, m. Also, δ_u is 0.024 m.

Therefore, the total thermal resistance of the model is shown in the following equation:

$$R = \frac{1}{(1/R1 + 1/R2 + 1/R3)}, \tag{5}$$

where R is the total thermal resistance of the model, °C/W.

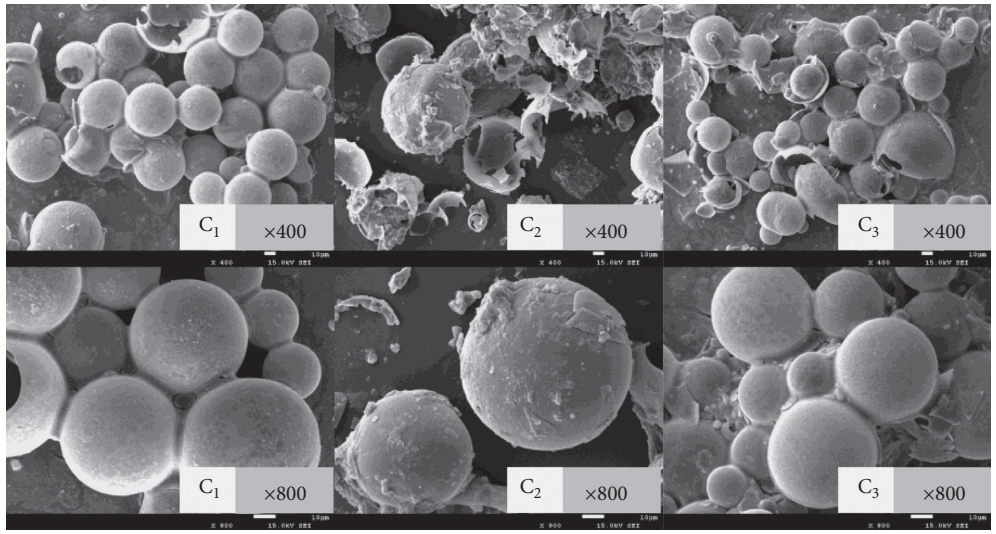

Figure 11: SEM tests of the three HGM composites.

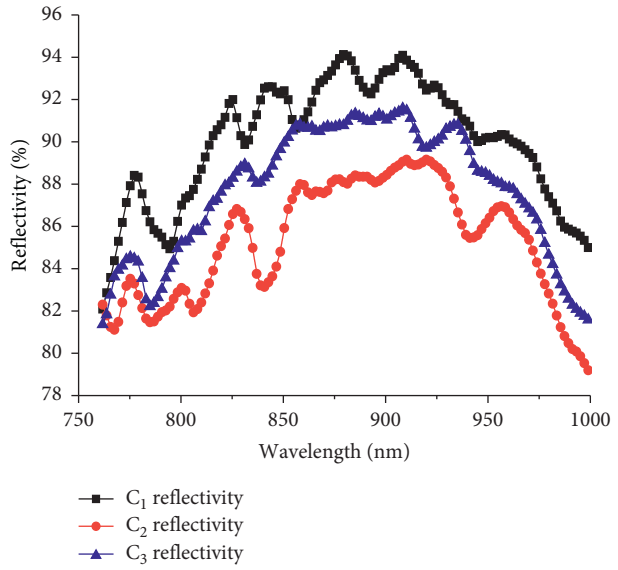

Figure 12: Infrared reflectance of the hollow microspheres.

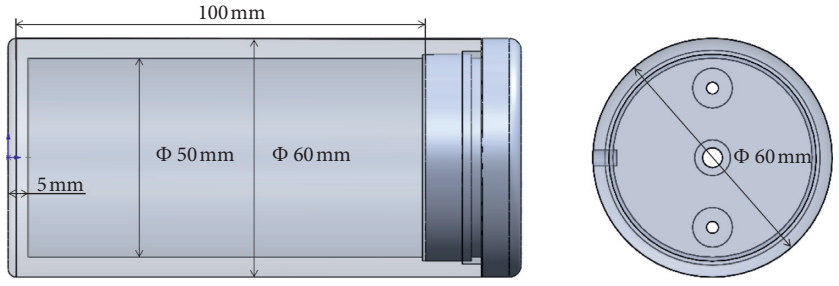

Figure 13: Small test cabin.

Assuming that the liquid temperature in the test cabin is $T(t)$ at any moment, equation (6) can be obtained. The left side of the equation is the heat energy consumed by the liquid to heat up, and the right side of the equation is based on flat wall heat transfer, and the fraction represents the process of heat transfer, which is called Ohm's law in electricity.

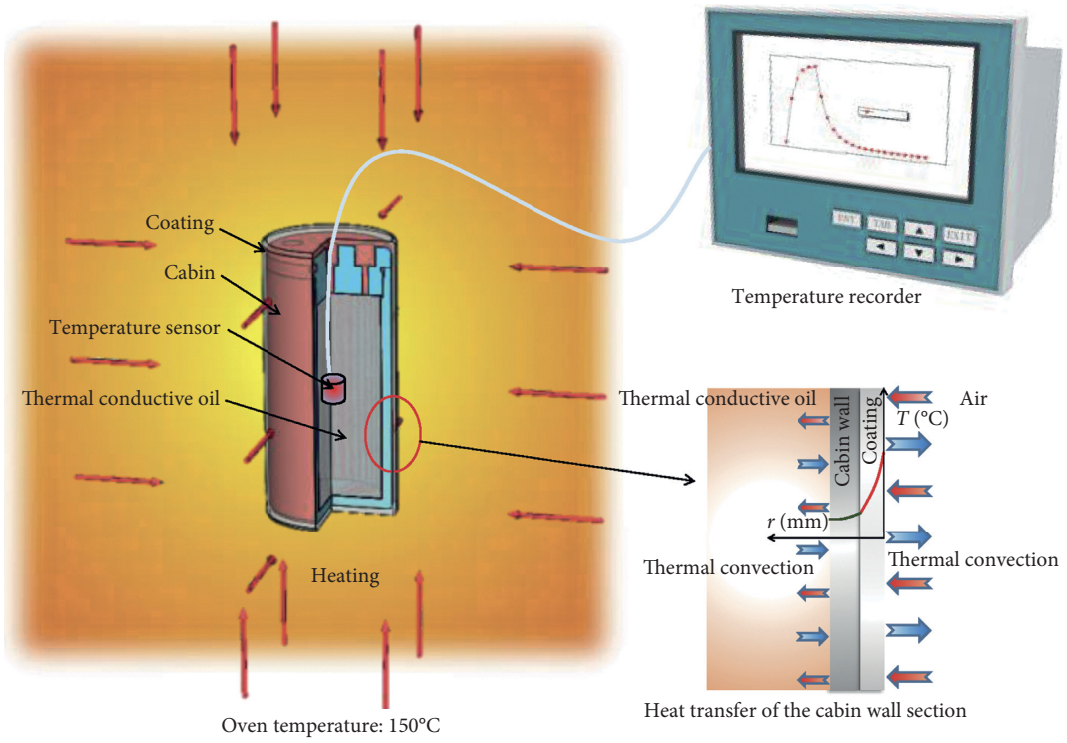

Figure 14: Passive thermal insulation material effectiveness test.

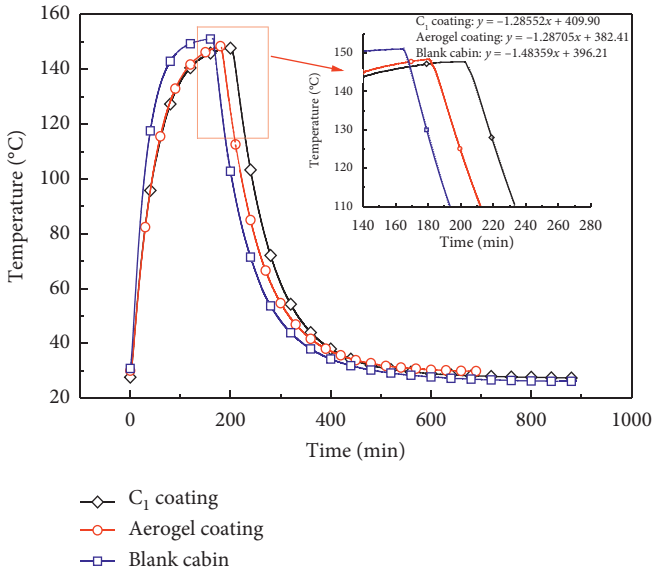

Figure 15: Effective test results of the passive thermal insulation material.

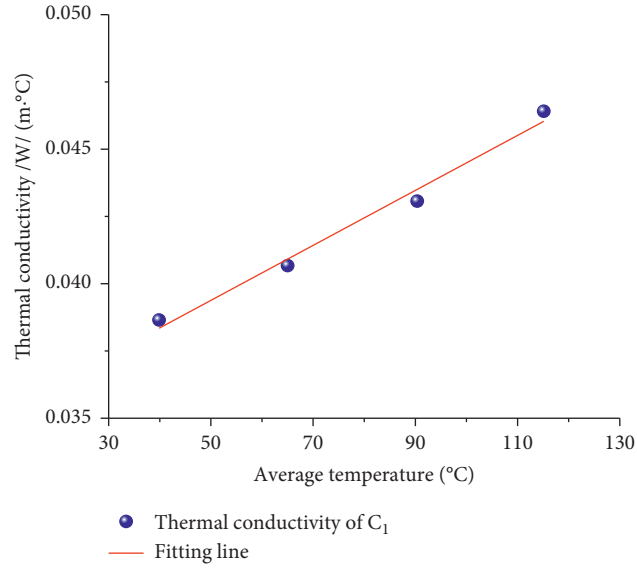

Figure 16: Thermal conductivity of the C_1 material at different temperatures.

$$m_w c_w (T_0 - T(t)) = \int \frac{T(t) - T_a}{R} dt, \quad (6)$$

where m_w is the liquid mass in the cabin, kg; c_w is the liquid specific heat capacity, J/(kg·°C); $T(t)$ and T_0 are the temperature at any moment and the initial temperature of the liquid, respectively, °C; and T_0 is the ambient temperature, °C.

Finally, the fluid temperature at any moment can be obtained, as shown in the following equation:

$$T(t) = e^{\left[-\left(1/m_w c_w R\right)t + \ln\left(T_0 - T_a\right)\right]} + T_a. \quad (7)$$

According to equation (1), the thermal conductivity of the C_1 material can be averaged at 0.04321 W/(m·°C) during the cooling process. In the case where the initial temperature of the inner fluid is 150°C, it is assumed that the ambient

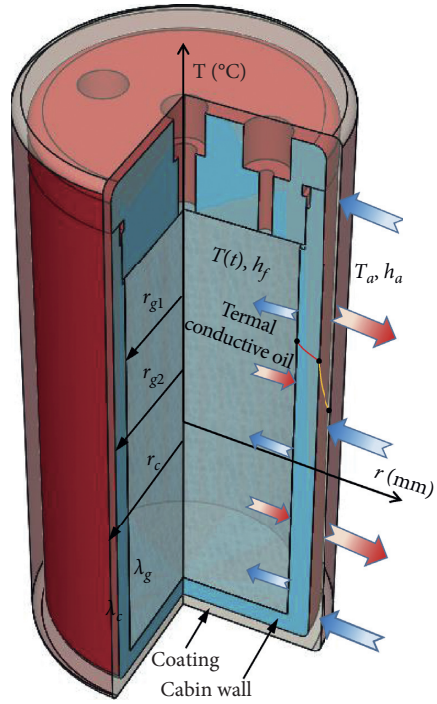

Figure 17: Simplified model of the small test cabin.

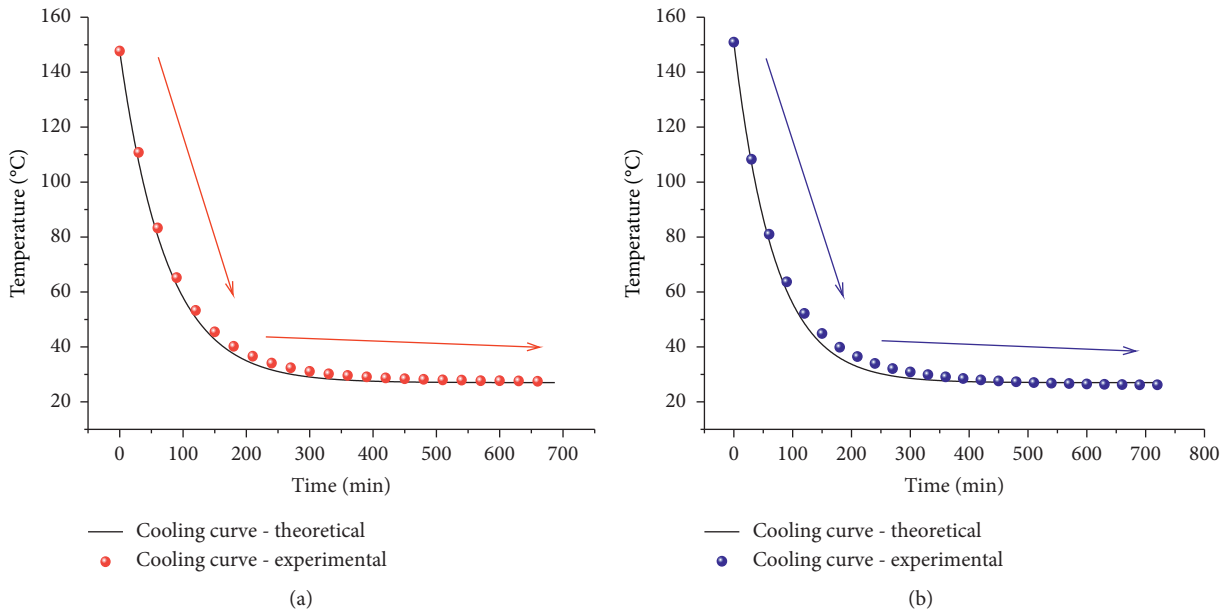

Figure 18: Comparison of the experimental and theoretical cooling curves. (a) Results of the cabin covered with C_1. (b) Results of the blank cabin.

temperature is 25°C. Therefore, according to the test cabin size, the theoretical cooling curves of C_1 and the blank can be obtained, as shown in Figure 18.

As shown in Figure 18, the theoretical cooling curve is in good agreement with the test results. Additionally, the relevant parameters can be substituted into equations (3)–(6) to obtain the heat transfer model of the actual core cabin, thereby providing guidance for engineering applications. In addition, the cooling process of the cabin is mainly divided into two stages. In the initial cooling stage, the cooling rate is faster, which is caused by the large temperature difference between the interior of the cabin and the ambient environment. This observation corresponds to the increasing temperature difference between the inside and

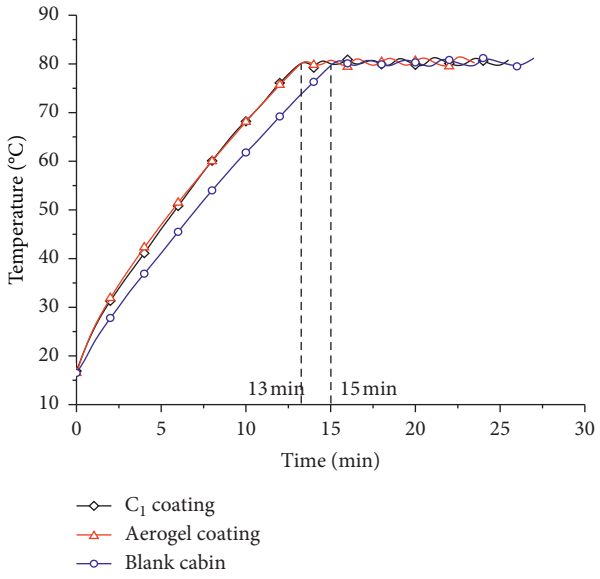

Figure 19: Integration test results of the thermally insulated coring system.

outside of the cabin when lifting the corer out of the ground. In the second stage, the temperature difference is small, the cooling rate gradually decreases, and the temperature inside the cabin eventually approaches room temperature. This shows that active thermal insulation should provide more temperature compensation when the temperature difference is large, which can reduce energy consumption.

6.2. Validation Test for the Integration of the Thermally Insulated Coring Test System. To validate the scheme of a combined active and passive thermal insulation system, an integration test was carried out. To be close to actual operating conditions, a 12 V power supply was used.

The chosen passive insulation materials were the C_1 and SiO_2 aerogel coatings; there was also a blank cabin. The graphene heating material was used to heat water from room temperature to 80°C and, then, kept at a constant temperature; the temperature change was recorded.

As shown in Figure 19, the passive insulation materials effectively reduce the heat loss during the heating process. The two test cabins with thermal insulation materials take 13 min and consume 84262.46 J when the temperature is raised to 80°C, while the blank cabin takes 15 min and consumes 97225.92 J. Therefore, combined with the passive thermal insulation measures, active thermal insulation can increase the insulation effect by 13.3% in terms of time and energy consumption, effectively retaining the in situ temperature of the core and reducing energy consumption. At the constant temperature stage, due to the effect of the PID chip, the water temperature fluctuates around 80°C, and a small fluctuation amplitude can be achieved by adjusting the PID accuracy. Overall, the test results verify the feasibility of the thermally insulated coring system.

According to the test results, the thermal insulation method of the coring system can adopt the concept of active thermal insulation (graphene heating material) and combine it with a passive thermal insulation material (C_1). Engineering applications also need to consider the layout of the circuit, graphene materials, and C_1 in the corer. Then, according to the working conditions, thermally insulated deep rock coring equipment can be designed.

7. Conclusions

A deep rock corer that retains the insitu temperature of the core consists of active and passive thermal insulation. A scheme was designed, and experiments were performed to obtain the following conclusions:

(1) Temperature sensors recorded the core temperature in the active insulation scheme design and provided feedback to the PID chip controls, so the heating material could instantly compensate for changes in the core temperature. The graphene heating material had low thermal inertia, which shortened the heating time by 28.5 min and saved the consumption of 32198.94 J. Therefore, the graphene heating material was chosen in the active insulation scheme.

(2) A passive insulation material with low thermal conductivity decreases the temperature loss of the core. For the hollow microsphere coating and aerogel felt, insulation property tests were performed, and the results showed that C_1 had better insulation properties and the highest infrared reflectance (90.02%), so the C_1 material could be used as a passive thermal insulation material.

(3) A passive insulation heat transfer model was established, and the passive insulation test results were verified, which will provide guidance for the development of integrated thermal insulation systems and engineering applications of deep rock corers.

(4) With the combination of active and passive insulation schemes, integrated insulation system tests were conducted. Compared with the blank control group, the integrated insulation system showed a decrease of 13.3% in terms of time and energy consumption. Thus, the test results verified the feasibility of the insulation system.

Data Availability

The raw/processed data required to reproduce these findings cannot be shared at this time as the data also form part of an ongoing study.

Conflicts of Interest

The authors declare that they have no conflicts of interest.

Acknowledgments

This study was funded by the National Natural Science Foundation of China (Grant nos. 51822403 and 51827901)

and the Sichuan International Technological Innovation Cooperation Project (Grant no. 2018HH0159).

References

[1] H. P. Xie, F. Gao, and Y. Ju, "Research and development of rock mechanics in deep ground engineering," *Chinese Journal of Rock Mechanics and Engineering*, vol. 34, no. 11, pp. 2161–2178, 2015.

[2] M. Z. Gao, S. Zhang, J. Li et al., "Dynamic failure mechanism of coal and gas outbursts and response mechanism of support structure," *Thermal Science*, vol. 23, p. 122, 2019.

[3] H. P. Xie, F. Gao, Y. Ju et al., "Quantitative definition and investigation of deep mining," *Journal of China Coal Society*, vol. 40, no. 1, pp. 1–10, 2015.

[4] H. P. Xie, "Research framework and anticipated results of deep rock mechanics and mining theory," *Advanced Engineering Sciences*, vol. 49, no. 2, pp. 1–16, 2017.

[5] M. Z. Gao, R. Zhang, J. Xie, G. Y. Peng, B. Yu, and P. G. Ranjith, "Field experiments on fracture evolution and correlations between connectivity and abutment pressure under top coal caving conditions," *International Journal of Rock Mechanics and Mining Sciences*, vol. 111, pp. 84–93, 2018.

[6] M. Gao, Z. Zhang, Y. Xiangang, C. Xu, Q. Liu, and H. Chen, "The location optimum and permeability-enhancing effect of a low-level shield rock roadway," *Rock Mechanics and Rock Engineering*, vol. 51, no. 9, pp. 2935–2948, 2018.

[7] C. Zhu, L. Wang, X. Han et al., "State judgement model of the coal and rock medium and its engineering application," *Advances in Civil Engineering*, vol. 2020, pp. 1–11, 2020.

[8] L. Chen, Y. Chu, Y. Zhang, F. Han, and J. Zhang, "Analysis of heat transfer characteristics of fractured surrounding rock in deep underground spaces," *Mathematical Problems in Engineering*, vol. 2019, pp. 1–9, 2019.

[9] F. Q. Gong, X. F. Si, X. B. Li, and S. Y. Wang, "Experimental investigation of strain rockburst in circular caverns under deep three-dimensional high-stress conditions," *Rock Mechanics and Rock Engineering*, vol. 52, no. 5, pp. 1459–1474, 2019.

[10] F. Q. Gong, W. X. Wu, T. B. Li et al., "Experimental simulation and investigation of spalling failure of rectangular tunnel under different three-dimensional stress states," *International Journal of Rock Mechanics and Mining Science*, vol. 122, Article ID 104081, 2019.

[11] S. M. Liu, X. L. Li, D. K. Wang et al., "Mechanical and acoustic emission characteristics of coal at temperature impact," *Natural Resources Research*, vol. 4, 2019.

[12] X. J. Liao, C. B. Jiang, M. K. Duan et al., "Influence of temperature on the mechanical and deformation properties of containing-gas raw coal under mining," *Journal of Northeastern University*, vol. 38, no. 9, pp. 1347–1352, 2017.

[13] C. Wang, M. He, X. Zhang, Z. Liu, and T. Zhao, "Temperature influence on macro-mechanics parameter of intact coal sample containing original gas from baijiao coal mine in china," *International Journal of Mining Science and Technology*, vol. 23, no. 4, pp. 597–602, 2013.

[14] J. Xu, D. D. Zhang, S. J. Peng et al., "Experimental research on influence of temperature on mechanical properties of coal containing methane," *Chinese Journal of Rock Mechanics and Engineering*, vol. 30, no. s1, pp. 2730–2735, 2011.

[15] M. C. He, C. G. Wang, D. J. Li et al., "Desorption characteristics of adsorbed gas in coal samples under coupling temperature and uniaxial compression," *Chinese Journal of Rock Mechanics and Engineering*, vol. 29, no. 5, pp. 865–872, 2010.

[16] C. G. Wang, L. J. Chen, C. S. Wang et al., "Experiment on thermal-induced expansion and mechanical properties of gas-bearing intact coal subjected to thermal-mechanical loading," *Rock and Soil Mechanics*, vol. 35, no. 4, pp. 1015–1024, 2014.

[17] C. Guan, S. Liu, C. Li, Y. Wang, and Y. Zhao, "The temperature effect on the methane and CO2 adsorption capacities of Illinois coal," *Fuel*, vol. 211, pp. 241–250, 2018.

[18] S. Richard, D. Stuart, W. Steve et al., "Temperature dependence of sorption of gases by coals and charcoals," *International Journal of Coal Geology*, vol. 73, no. 3, pp. 250–258, 2008.

[19] Z. Q. Li, X. F. Xian, and Q. M. Long, "Experiment study of coal permeability under different temperature and stress," *Journal of China University of Mining and Technology*, vol. 38, no. 4, pp. 523–527, 2009.

[20] G. Z. Yin, C. B. Jiang, J. G. Wang et al., "Combined effect of stress, pore pressure and temperature on methane permeability in anthracite coal: an experimental study," *Transport in Porous Media*, vol. 100, no. 1, pp. 1–16, 2013.

[21] Z. J. Feng, Z. J. Wan, Y. S. Zhao et al., "Experimental study of permeability of anthracite and gas coal masses under high temperature and triaxial stress," *Chinese Journal of Rock Mechanics and Engineering*, vol. 29, no. 4, pp. 689–696, 2010.

[22] R. G. Rothwell and F. R. Rack, "New techniques in sediment core analysis: an introduction," *Geological Society, London, Special Publications*, vol. 267, no. 1, pp. 1–29, 2006.

[23] F. Abegg, H.-J. Hohnberg, T. Pape, G. Bohrmann, and J. Freitag, "Development and application of pressure-core-sampling systems for the investigation of gas- and gas-hydrate-bearing sediments," *Deep Sea Research Part I: Oceanographic Research Papers*, vol. 55, no. 11, pp. 1590–1599, 2008.

[24] H. Zhu, Q. Liu, J. Deng et al., "Pressure and temperature preservation techniques for gas-hydrate-bearing sediments sampling," *Energy*, vol. 36, no. 7, pp. 4542–4551, 2011.

[25] I. Norihito and Y. Koji, "Data report: hybrid pressure coring system tool review and summary of recovery result from gas-hydrate related coring in the Nankai Project," *Marine and Petroleum Geology*, vol. 66, pp. 323–345, 2015.

[26] H. Takahashi and Y. Tsuji, "Multi-well exploration program in 2004 for natural hydrate in the nankai-trough offshore Japan," in *Proceedings of the Offshore Technology Conference*, Houstan, TX, USA, May 2005.

[27] H. Y. Zhu, Q. Y. Liu, G. R. Wong et al., "A pressure and temperature preservation system for gas-hydrate-bearing sediments sampler," *Petroleum Science and Technology*, vol. 31, no. 6, pp. 652–662, 2013.

[28] H. W. Qin, L. Y. Gu, S. L. Li et al., "Pressure tight piston corer-A new approach on gas hydrate investigation," *China Ocean Engineering*, vol. 19, no. 1, pp. 121–128, 2005.

[29] Y. Chen, H. W. Qin, S. L. Li et al., "Research on pressure tight sampling technique of deep-sea shallow sediment—a new approach to gas hydrate investigation % J China ocean engineering," *China Ocean Engineering*, vol. 20, no. 4, pp. 657–664, 2006.

[30] S. L. Li, Y. Cheng, H. W. Qin et al., "Development of pressure piston corer for exploring natural gas hydrates," *Journal of Zhejiang University (Engineering Science)*, vol. 40, no. 5, 2006.

[31] H. P. Xie, M. Z. Gao, R. Zhang et al., "Study on concept and progress of in situ fidelity coring of deep rocks," *Chinese Journal of Rock Mechanics and Engineering*, vol. 39, no. 5, pp. 865–876, 2020.

[32] Y. J. Dai, Y. Q. Tang, W. Z. Fang et al., "A theoretical model for the effective thermal conductivity of silica aerogel composites," *Applied Thermal Engineering*, vol. 128, 2018.

[33] G. S. Wei, Y. S. Liu, X. X. Zhang et al., "Thermal conductivities study on silica aerogel and its composite insulation materials," *International Journal of Heat and Mass Transfer*, vol. 54, no. 11-12, pp. 2355–2366, 2011.
[34] X. R. Song and H. Yang, "Development on preparation technology of hollow glass microspheres," *Journal of the Chinese Ceramic Society*, vol. 40, no. 3, pp. 450–457, 2012.
[35] Y. Hu, R. Mei, Z. An, and J. Zhang, "Silicon rubber/hollow glass microsphere composites: influence of broken hollow glass microsphere on mechanical and thermal insulation property," *Composites Science and Technology*, vol. 79, pp. 64–69, 2013.
[36] J. Z. Liang and F. H. Li, "Heat transfer in polymer composites filled with inorganic hollow micro-spheres: a theoretical model," *Polymer Testing*, vol. 26, no. 8, pp. 1025–1030, 2007.
[37] B. Li, J. Yuan, Z. An, and J. Zhang, "Effect of microstructure and physical parameters of hollow glass microsphere on insulation performance," *Materials Letters*, vol. 65, no. 12, pp. 1992–1994, 2011.
[38] S. M. Yang and W. Q. Tao, *Heat Transfer*, Higher Education Press, Beijing, China, 4 edition, 2006.